Microgravity Sci. Technol. (2015) 27:39–47
DOI 10.1007/s12217-014-9411-z

ORIGINAL ARTICLE

Free Surface Deformation of Thermo-Solutocapillary Convection in Axisymmetric Liquid Bridge

Xiaoming Zhou · Xiulan Huai

Received: 18 August 2014 / Accepted: 16 December 2014 / Published online: 31 December 2014

Abstract Steady thermo-solutocapillary convection in axisymmetric liquid bridge with dynamic free surface is numerically studied in the absence of gravitational effects. The upper and lower disks of liquid bridge maintain at constant temperature and solute concentration. The deformable free surface is obtained by Level set method. Numerical simulations are carried out for Prantle number $Pr = 1$, Capillary number $Ca = 0.1$, Marangoni number $1 \leq Ma \leq 100$, and thermal to solutal Marangoni number ratio $-10 \leq R_\sigma \leq 0.1$. The results show that there are three modes of free surface deformation in thermo-solutocapillary convection under low Marangoni number: 1) as $-10 \leq R_\sigma < -1$, the free surface bulges out near the lower disk and bulges in near the upper disk; 2) as $R_\sigma = -1$ the free surface bulges out near the lower and upper disks and bulges in at the central region of the liquid bridge; 3) as$-1 R_\sigma \leq -0.1$, the free surface bulges out near the upper disk and bulges in near the lower disk. Moreover, the effect of Marangoni number on free surface deformation also is discussed.

Keywords Thermo-solutocapillary convection · Liquid bridge · Free surface · Level set method · Marangoni number

X. Zhou (✉) · X. Huai
Institute of Engineering Thermal Physics,
Chinese Academy of Sciences, Beijing, 100190, China
e-mail: xmzhou@iet.cn

X. Huai
e-mail: hxl@iet.cn

Introduction

Thermo-solutocapillary convection is driven by surface tension gradient due to the variation of temperature and solute concentration at free surface. This phenomenon widely exists in crystal growth process, welting process, and many other industrial processes. The most widely studied model associated with the thermo-solutocapillary convection is a liquid bridge with temperature and solute concentration differences between two disks. As early as 1969, Levich and Krylov (1969) had made an analysis of the coupling of thermocapillary convection and solutocapillary convection. The first time numerical investigation of thermo-solutocapillary convection in liquid bridge or float zone is by You and Hu (1992), they found that the solutal Marangoni number has obvious influence on the streamline function and the solute distribution but has relatively slight effect on the temperature distribution. Wanschura et al. (1995) made a linear stability analysis of thermo- and solutocapillary convection in a cylindrical liquid bridge, and they obtained critical Reynolds numbers for different parameter variations. Artemyev et al. (2001) numerically investigated the heat mass transfer processes in germanium crystal growth by the floating zone method under microgravity conditions, the thermal and solutal kinds of Marangoni convection in the molten zone was considered. Walker et al. (2002) numerically investigated the thermo-solutocapillary convection under a strong magnetic field. Joly et al. (2004) investigated the transport dynamics and stability limit of the axisymmetric steady flow driven by a surface tension variation in a liquid bridge configuration, in which the thermal and solutal Marangoni effect were

included. Minakuchi et al. (2004) numerically studied the effect of solutal Marangoni convection during the Si_xGe_{1-x} crystal growth by the floating-zone technique under zero gravity, the results show that the contribution of the solutal Marangoni convection to the flow structure was significant although the strength of the solutal Marangoni convection is much weaker than that of the thermal Marangoni convection. Lin et al. (2005) numerically investigated Marangoni flows in a floating zone of germanium-silicon crystals, the competition between the thermocapillary and solutocapillary flows in the floating zones was qualitatively examined, and in their model the static deformable free surface was used. Lyubimova et al. (2007a, b; 2011a, b) made a lot of investigation on thermo-solutocapillary convection in float zone crystal growth, they studied the flow structure and flow instability of the convection, and obtained the effect of constant axial magnetic field on the thermosolutocapillary convection Recently, Minakuchi et al. (2012, 2014) studied the thermo-solutal Marangoni convection occurring in a liquid bridge of a silicon-germanium system under zero gravity, and they also investigated the relative contributions of thermal and solutal Marangoni convections on transport structures in a liquid bridge under zero gravity.

The literatures show that the thermo-solutocapillary convection in liquid bridge or float zone has been investigated extensively, however, all the above studies were dedicated to the situation of nondeformable free surface or static deformable free surface, and the dynamic deformation of free surface was neglected in order to avoid the simulation complexity associated with the unknown free surface shapes. It is well known that the deformation of free surface has an important influence on the pure thermocapillary convection, in particular for the onset of the oscillatory flow in liquid bridge (Sim et. al 2004). Microgravity experiment by Koster (1994) indicated that, a detailed investigation of thermocapillary convection in multilayered fluid systems needed to take account for finite interface deformations in conjunction with a suitable dynamic contact line condition. Moreover, the dynamic deformation of free surface in pure thermocapillary convection of liquid bridge has been considered by many investigators (Kuhlmann and Nienhuser (2002); Kawajia et al. (2006); Liang et al. (2014)).

To the authors' knowledge, the dynamic deformation of free surface in the numerical simulation of thermo-solutocapillary convection has not been considered. Therefore, in the present work we report on the simulations of steady thermo-solutocapillary convection with a deformable free surface in axisymmetric liquid bridge by level set method, and the effects of thermal to solutal Marangoni number ratio and Marangoni number on the thermo-solutocapillary convection are discussed.

Physical and Mathematical Models

The liquid bridge with radius R_0 and height H is suspended between two coaxial disks and surrounded by the gas in a cylindrical container with radius $2R_0$ and height H as shown in Fig. 1. The Aspect ratio of the liquid bridge is $A=H/R_0 = 1.2$. The liquid bridge is filled with a binary fluid, which is a two-component mixture working medium. The interface between the fluid and gas is a deformable free surface. Different temperatures and concentrations are applied at the upper disk (T_1, C_1) and lower disk (T_2, C_2), where $T_1 > T_2$ and $C_1 > C_2$. The no-slip boundary condition is adopted for the upper and lower disks, and the surface tension force acts on the free surface. All the thermal properties are assumed to be constant except for the surface tension, and the surface tension is allowed to vary linearly with the liquid temperature and solute concentration. Thus the surface tension can be formulated as,

$$\sigma = \sigma_0 - \gamma_T (T - T_0) - \gamma_C (C - C_0)$$

where $\sigma_0 = \sigma(T_0, C_0)$, $\gamma_T = -(\partial\sigma/\partial T)$, $\gamma_C = -(\partial\sigma/\partial C)_T$. Thermophysical properties of the fluid are estimated at the reference temperature T_0 and concentration C_0, which are set to be equal to T_1 and C_1, respectively. Moreover, only the liquid surface tension increases with concentration and decreases with temperature are considered. The fluid flow is assumed to be laminar, and buoyancy effects are neglected in present study.

The nondimensional variables of velocity, temperature, solute concentration, coordinates, time and pressure are defined as $V = \frac{u}{U}, \Theta = \frac{T-T_1}{T_2-T_1}, C^* = \frac{C-C_1}{C_2-C_1}, (R, Z) = \frac{(r,z)}{R_0}, \tau = \frac{tU}{R_0}, P = p/(\rho_l U^2)$, respectively. Here, $U = \gamma_T \Delta T/\mu_l$ is characteristic velocity. The level set method

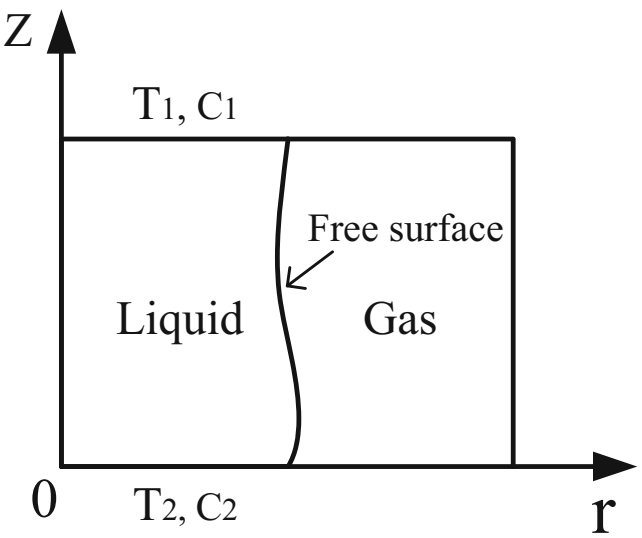

Fig. 1 Physical model

is employed to capture the free surface implicitly by introducing a smooth level set function, with the zero level set as the free surface, positive value outside the free surface, and negative value inside the free surface. Then, the non-dimensional Navier-Stokes equations governing the thermo-solutocapillary convection are expressed as follows:

$$\nabla \cdot \boldsymbol{V} = 0 \tag{1}$$

$$\begin{aligned}\frac{\partial \boldsymbol{V}}{\partial \tau} + \nabla \cdot (\boldsymbol{VV}) = & -\frac{1}{\tilde{\rho}}\nabla P + \frac{1}{\tilde{\rho} Re}\nabla \cdot (\tilde{\mu}\nabla \boldsymbol{V}) \\ & + \frac{1}{\tilde{\rho} Re}\nabla \cdot (\tilde{\mu}\nabla \boldsymbol{V})^T + \frac{1}{\tilde{\rho} Re}\left(\nabla_s \Theta + \frac{\nabla_s C^*}{R_\sigma}\right)\delta(\phi) \\ & + \frac{1}{\tilde{\rho} Re}\left(\frac{1}{Ca} + \Theta + \frac{C^*}{R_\sigma}\right)\frac{k(\phi)\delta(\phi)\nabla\phi}{\tilde{\rho}}\end{aligned} \tag{2}$$

$$\frac{\partial \Theta}{\partial \tau} + \boldsymbol{V} \cdot \nabla \Theta = \frac{1}{\tilde{\rho}\tilde{C}_p Ma}\nabla \cdot (\tilde{\lambda}\nabla \Theta) \tag{3}$$

$$\frac{\partial \mathrm{C}^*}{\partial \tau} + \boldsymbol{V} \cdot \nabla C^* = \frac{1}{LeMa}\nabla \cdot (\tilde{\mathrm{D}}\nabla C^*) \tag{4}$$

$$\frac{\partial \phi}{\partial \tau} + \boldsymbol{V} \cdot \nabla \phi = 0 \tag{5}$$

where $\tilde{\mu} = \mu/\mu_l$, $\tilde{\rho} = \rho/\rho_l$, $\tilde{\lambda} = \lambda/\lambda_l$, $\tilde{D} = D/D_l$ and $\tilde{C}_p = C_p/C_{pl}$ are the dimensionless viscosity, density, thermal conductivity, solute diffusivity, and specific heat, respectively. ϕ is the Level set function, δ is the smeared-out Dirac delta function, and $\nabla_s = (\boldsymbol{I} - \boldsymbol{nn}) \cdot \nabla$ is free surface gradient operator. The dimensionless parameters are defined as follows: thermal Marangoni number $Ma_T = \frac{\gamma_T \Delta T R_0}{\mu_l \alpha_l}$, Solutal Marangoni number $Ma_C = \frac{\gamma_C \Delta C R_0}{\mu_l \alpha_l}$, Marangoni number $Ma = |\mathrm{Ma_T}|$, Reynolds number $Re = \frac{U R_0}{\nu_l}$, Capillary number $Ca = |Ca_\mathrm{T}\ \mathrm{Ca_C}|$, $\mathrm{Ca_T} = \frac{\gamma_T \cdot \Delta T}{\sigma_0}$ and $\mathrm{Ca_C} = \frac{\gamma_c \cdot \Delta C}{\sigma_0}$, the ratio of thermal Marangoni number to solutal Marangoni $R_\sigma = \frac{\gamma_T \cdot \Delta T}{\gamma_C \cdot \Delta C}$, Prandtl number $\mathrm{Pr} = \frac{\nu_l}{\alpha_l}$ and Lewis number $\mathrm{Le} = \frac{\alpha_l}{D_l}$. The Marangoni number equals to the product of Reynolds number and Prandtl number, namely Ma = Pr*Re. The subscripts of g and l note the gas and liquid, respectively. The continuum surface force (CSF) model (Brackbill et al. 1992) is used to reformulate the surface tension as a volume force, and the fourth and fifth terms at the right hand of the momentum equation are the tangential and normal surface tension, respectively.

The corresponding physical variants can be expressed as

$$\begin{aligned}\tilde{\rho} &= \eta_\rho + (1 - \eta_\rho)H(\phi), \\ \tilde{\mu} &= \eta_\mu + (1 - \eta_\mu)H(\phi)\end{aligned} \tag{6}$$

where $\eta_\rho = \rho_\mathrm{g}/\rho_l$, $\eta_\mu = \mu_g/\mu_l$, $H(\phi)$ is the smeared-out Heaviside function defined by

$$H(\phi) = \begin{cases} 1 & \phi < -\xi \\ \frac{1}{2} + \frac{\phi}{2\xi} + \frac{1}{2\pi} sin\left(\frac{\pi\phi}{\xi}\right) & -\xi \le \phi \le \xi \\ 0 & \phi > \xi \end{cases} \tag{7}$$

where ξ is a tunable parameter that determines the size of the bandwidth of numerical smearing. A typical good value is $\xi = 1.5\Delta R$, and ΔR is the grid step spacing in R-direction

To keep the level set function as a distance function from the front, an approach based on solving the hyperbolic partial differential equation has been presented in reference (Sussman et al. 1994). The reinitialization equation is

$$\phi_Y = sign\,(\phi_0)\,(1 - |\nabla\phi|)\,, \quad \phi\,(R, 0) = \phi_0\,(R) \tag{8}$$

Where $|\nabla\phi| = \sqrt{\phi_R^2 + \phi_Z^2}$, and the sign function $sign_\xi\,(\phi_0) = \frac{\phi}{\sqrt{\phi^2 + \xi^2}}$.

Moreover, in order to make the total mass completely satisfy the mass conservation in time, the mass conserving procedure proposed by Liang et al. (2011) is used.

Boundary and Initial Conditions

$$\Theta = 0, C^* = 0, \boldsymbol{V} = 0, \frac{\partial \phi}{\partial \mathrm{Z}} = 0 \qquad \text{at } Z = 0 \tag{9-a}$$

$$\Theta = 1, C^* = 1, \boldsymbol{V} = 0, \frac{\partial \phi}{\partial Z} = 0 \qquad \text{at } Z = 1.2 \tag{9-b}$$

$$V_\mathrm{R} = 0, \frac{\partial \mathrm{V_Z}}{\partial \mathrm{R}} = 0, \frac{\partial \Theta}{\partial \mathrm{R}} = 0, \frac{\partial C^*}{\partial \mathrm{R}} = 0, \frac{\partial \phi}{\partial R} = 0 \quad \text{at } R = 0 \tag{9-c}$$

$$V_\mathrm{R} = 0, V_\mathrm{z} = 0, \frac{\partial \Theta}{\partial \mathrm{R}} = 0, \frac{\partial C^*}{\partial \mathrm{R}} = 0, \frac{\partial \phi}{\partial R} = 0 \quad \text{at } R = 2 \tag{9-d}$$

$$\Theta = 0, C^* = 0, \boldsymbol{V} = 0, \phi\,(1, Z) = 0, P = 0 \quad \text{at } \tau = 0 \tag{9-e}$$

In this paper, we consider the contact conditions of interface with the upper and lower disks is contact points fixed.

Computational Method

In this article we use the Runge-Kutta Crank-Nicholson (RKCN) projection method presented by Ni et al. (2003) to solve the governing equations The Crank-Nicholson implicit technique is employed to update the diffusion term, and the low storage three-stage Runge-Kutta technique is employed to update the convective term. This

method has second-order temporal accuracy for variable-density unsteady incompressible flows. The diffusion term in momentum equation is discretized using standard central difference schemes, while the convective term is discretized by high-order compact schemes. The convective term in the level set equation using the third-order essentially nonoscillatory (ENO) scheme. The non-dimensional time step for all the simulations is 1×10^{-3}. This detailed description of the computational method can refer to our previous paper (Zhou and Huang 2010) The numerical code is validated by comparing computed surface deformation of pure thermocapillary convection with those from Sim et al. (2004) in Fig. 2. The parameters for the simulation are Pr =1, A = 1, Ca = 0.05 and Re = 1 The numerical results at Bi = are in good agreement with Sim's results

The axisymmetric liquid bridge is discretized with a uniform mesh, and this mesh is determined by refining the mesh size until convergence and constancy of flow velocity, temperature, concentration and free surface deformation is achieved. The grid number $200^{R_*}200^{Z}$ is used, which is found to be sufficient to accurately capture the free surface, temperature, solute concentration and flow fields.

Results and Discussions

In the liquid bridge, both the temperature and solute concentration differences between the upper and lower disks produce a surface tension gradient at free surface, so the thermocapillary and solutocapillary convection can be induced. The numerical simulations are carried out for Prandtl number Pr = 1, Lewis number Le = 100, Capillary number Ca = 0.1, Marangoni number $1 \leq \mathrm{Ma} \leq 100$ and thermal to solutal Marangoni number ratio $-10 \leq R_\sigma \leq -0.1$. All the simulations start from the all-zero initial field $\boldsymbol{V} = P = \Theta = C^* = 0$ and the thermo-solutocapillary convection is considered to be fully developed as the velocity, temperature, solute concentration and free surface deformation keep constant in computational process, namely the final steady thermo-solutocapillary convection. The convergence criteria can be defined as follows: for each time step the quotient $Q = \frac{|\varphi^{n+1} - \varphi^n|}{|\varphi^n_{max}|}$ is calculated for all dependent variables in all grid points, and the index n+1 denotes a discrete point of time which follows the point of time n after a time step $\Delta\tau$. If $Q \leq 10^{-5}$ is valid for all variables in all grid points the thermo-solutocapillary convection is interpreted as a steady flow. In our simulations, the density ratio, dynamic viscosity ratio, thermal conductivity ratio, solute diffusivity ratio and specific heat ratio of gas and liquid are $\eta_\rho = 2 \times 10^{-4}$, $\eta_\mu = 3 \times 10^{-3}$, $\eta_\lambda = 10^{-3}$, $\eta_\mathrm{D} = 10^{-3}$ and $\eta_{C_p} = 5$, respectively. The initial shape of the free surface of liquid bridge is a vertical non-deformable plane, and the computational results at the time of $\tau = 500$ are given in the paper.

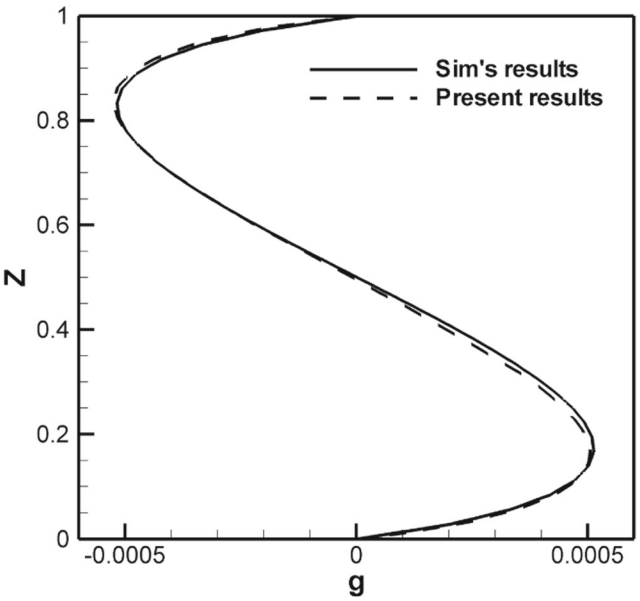

Fig. 2 Comparison of free surface deformation in liquid bridge with Sim's results

Influence of Thermal to Solutal Marangoni Number Ratio

The streamlines distribution of thermo-solutocapillary convection under different R_σ with Ca = 0.1, Le = 100, Ma = 1 is shown in Fig. 3, in which solid lines denote clockwise rotating cell and dashed lines denote anticlockwise rotating cell. As R_σ =-0.1, the flow field consists of one anticlockwise rotating convective cell, and from the fluid flow direction at free surface we can know that this convection is driven by solutocapillary effect. As $R_\sigma = -1$, the flow field consists of one anticlockwise and one clockwise rotating convective cells, and the lower and upper convective cells are driven by thermocapillary and solutocapillary effects, respectively. As $R_\sigma = -10$, the flow field consists of one clockwise rotating convective cell, which is driven by thermocapillary effect.

Figure 4 gives free surface deformations and surface pressure distribution under different R_σ with Ca = 0.1, Le = 100 and Ma = 1. It can be seen that the free surfaces is almost asymmetric about the central point (R = 1, Z = 0.6) of free surface. As $R_\sigma = -1$ the free surface deformation is very small, the order of magnitude is $O(10^{-6})$, whose amplified figure is shown in Fig. 4b. Meanwhile, the free surface bulges out near the lower and upper disks and bulges in at the central region of the liquid bridge. As $R_\sigma < -1$, the

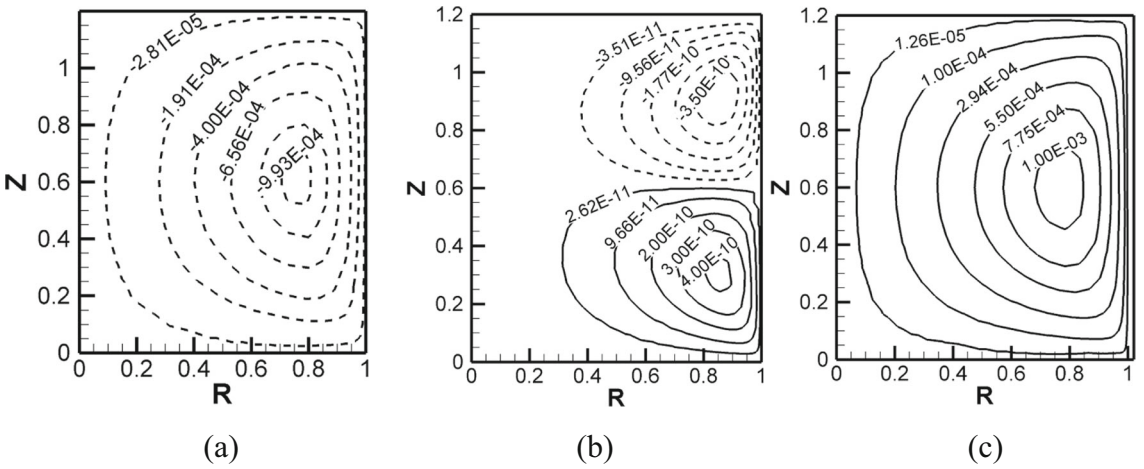

Fig. 3 Streamlines distribution with Ca=0.1, Le=100, Ma=1 and various R_σ

free surfaces bulge out near the lower disk and bulge in near the upper disk, and with the decrease of R_σ the free surface deformation increases. The surface deformation is $O(10^{-3})$, and its maximum value is 0.0011 at $R_\sigma = -10$, Ca = 0.1, Le = 100 and Ma = 1. As $R_\sigma > -1$, the free surfaces bulge out near the upper disk and bulge in near the lower disk, and the free surface deformation increases with the increase of R_σ. The free surface deformation is mainly caused by surface pressure gradient, so the mechanism of free surface deformation can be explained by the surface pressure distribution The corresponding surface pressure distribution of Fig. 4a is shown in Fig. 4c. As $R_\sigma = -1$, the surface pressure approximates to zero, this means the pressure gradient is zero, therefore this surface pressure distribution does not induce a obvious free surface deformation. As $R_\sigma < -1$, the surface pressure decreases along z axis, namely the

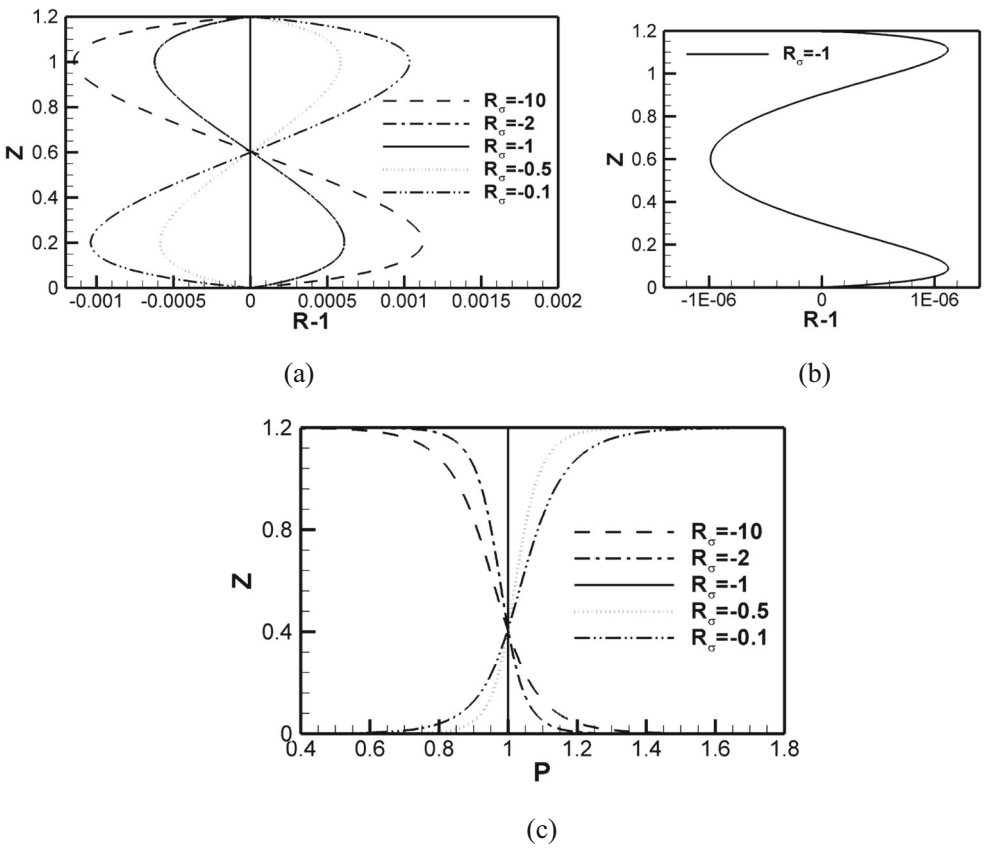

Fig. 4 Free surface deformations (**a**), amplified figure of R_σ =-1 (**b**) and surface pressure (**c**) distribution with Ca = 0.1, Le = 100, Ma = 1 and various R_σ

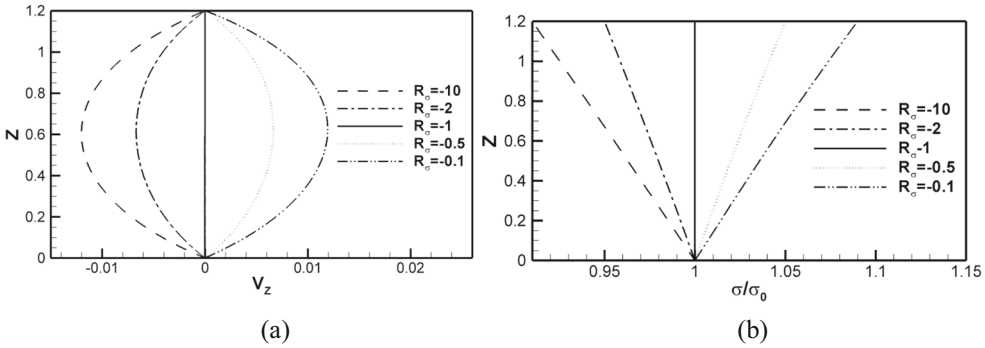

Fig. 5 Surface axial velocity (**a**) and surface tension (**b**) distribution with Ca = 0.1, Le = 100, Ma = 1 and various R_σ

pressure gradient is negative, this leads to the free surface bulges out near the lower disk. Meanwhile, the absolute pressure gradient increases with R_σ decreasing, so the free surface deformation increases with the decrease of R_σ. As $R_\sigma > -1$, the change tendency of surface pressure and pressure gradient along Z axis is opposite to that of $R_\sigma < -1$.

Figure 5 shows surface axial velocity distribution with Ca = 0.1, Le = 100, Ma = 1 and various R_σ. As $R_\sigma = -1$, the axial velocity is very small. As $R_\sigma < -1$, the surface axial velocity is negative, this means the free surface fluid flow from the upper disk to the lower disk, and it's magnitude increases with R_σ decreasing. As $R_\sigma > -1$, the surface axial velocity is positive, which means the free surface fluid flow from the lower disk to the upper disk, and it's magnitude increases with R_σ increasing. Figure 5b shows non-dimensional surface tension distribution under different R_σ with Ca = 0.1, Le = 100, and Ma = 1. As $R_\sigma = -1$, the non-dimensional surface tension is unit, this means that the thermocapillary forces is balanced by solutocapillary forces at free surface. As $R_\sigma < -1$, the non-dimensional surface tension is monotous decreasing, and it increases with R_σ decreasing. As $R_\sigma > -1$, the non-dimensional surface tension is monotous increasing, and it increases with R_σ increasing.

Influence of Marangoni Number

Figure 6 shows streamlines distribution under different Marangoni number with $R_\sigma = -1$, Ca = 0.1, Le = 100. As Ma = 1, the streamlines distribution is shown in Fig. 3b, the flow field consists of one anticlockwise and one clockwise rotating convective cells, and the size of the both cells are comparable. With Marangoni number increasing, the size of the lower convective cell increases, but that of the upper convective cell decreases. At the same time, the flow field is dominated by the lower cell, which is driven thermocapillary effect. This reason can be attributed to the thermal diffusivity is larger than that of mass diffusivity, which causes the convective cell driven by thermocapillary effect is formed before that driven by solutocapillary effect. Moreover, with Marangoni number increasing the temperature gradient is more quickly established across the surface and the clockwise rotating convective cell is generated, and this leads to the convective cell driven by solutocapillary effect is confined in the upper corner.

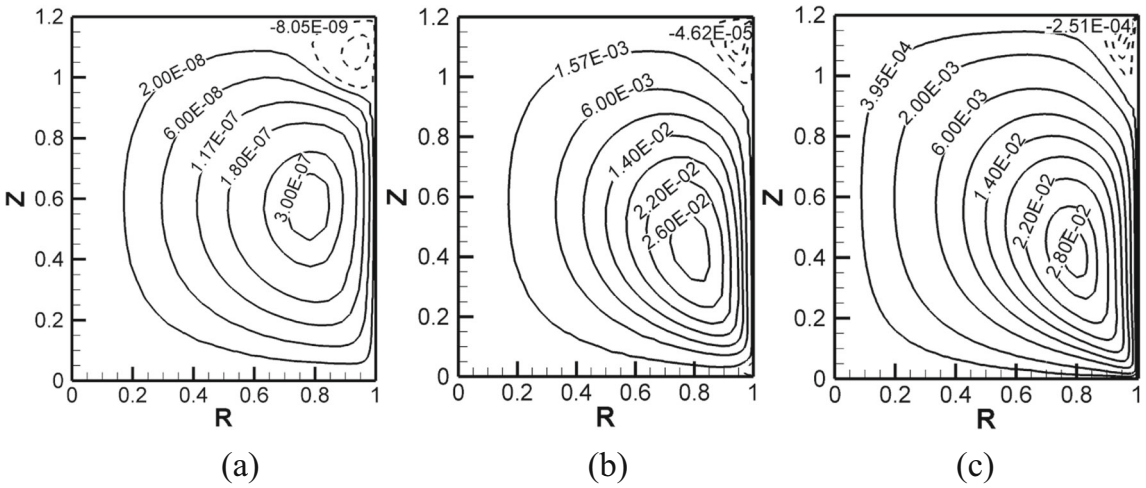

Fig. 6 Streamlines distribution with R_σ =-1, Ca = 0.1, Le = 100, and various Ma

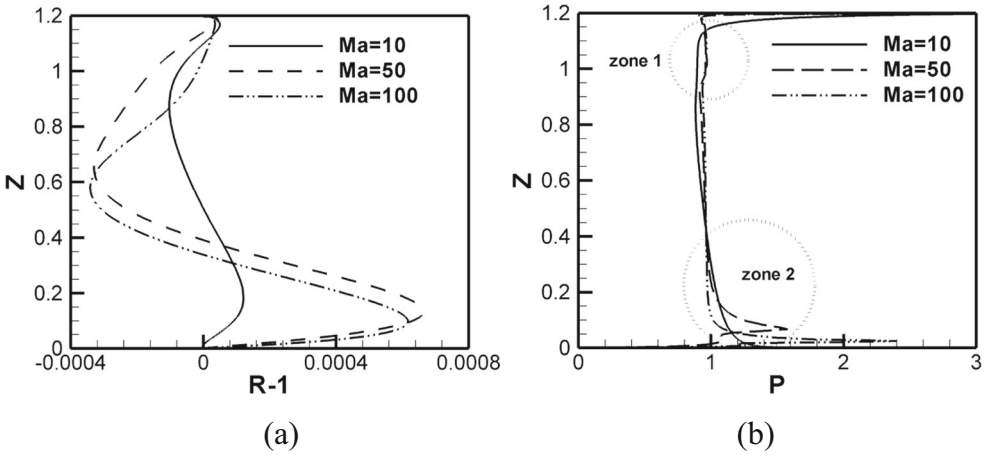

Fig. 7 Free surface deformations (**a**) and surface pressure (**b**) distribution with R_σ =-1, Le = 100, Ca = 0.1, and various Ma

Figure 7 shows free surface deformations and surface pressure distribution under various Marangoni numbers with $R_\sigma = -1$, Le = 100 and Ca = 0.1. We can see that the free surface deformations near the upper and lower disks almost equals to each other at $R_\sigma = -1$, Ma = 1, Le = 100 and Ca = 0.1, as shown in Fig. 4b. However, Fig. 7a shows that, as the Marangoni number increases the deformation near the lower disk increases deeply, but that near the upper disk decreases. Meanwhile, the maximal free surface deformation point travels to the lower disk, and the free surface deformation of Ma = 100 is less than that of Ma = 50. In Fig. 7b, the absolute value of pressure gradients at zone 1 and zone 2 is larger than that at the central region as Ma = 10, this leads to the free surface bulges out near the upper and lower disks. As Ma = 50 and 100, the obvious surface pressure gradient just occurs near the lower disk, this causes the free surface bulges out near the lower disk. Moreover, even if the pressure gradient near the lower disk of Ma = 100 is larger than that of Ma = 50, but the boundary effect of the lower dick damps the free surface deformation, which results in the free surface deformation in case Ma = 100 is smaller.

In the next, we shall discuss the effect of Marangoni number in the case of $R_\sigma = -10$. With the increase of Marangoni number the flow fields remain unchanged, and similar to Fig. 3c, so we do not give the flow fields under various Marangoni numbers here. Figure 8 shows free surface deformations and surface pressure with $R_\sigma = -10$, Le = 100, Ca = 0.1 and various Ma. For different Marangoni numbers, the free surfaces bulge out near the lower disk and bulge in near the upper disk. As Marangoni number increases, the free surface deformation near the upper disk is reduced, and the length between the maximal point and the minimal point also is reduced. Therefore, the free surface deformation is reduced with the increase of Marangoni number. The surface pressures distribution in Fig. 8b show that, the absolute of pressure gradient decreases with Marangoni number increasing, then results in the free surface deformation decreases.

Figure 9 shows surface axial velocity and surface tension distribution under various Marangoni numbers with $R_\sigma = -10$, Le = 100 and Ca = 0.1. With Marangoni number increasing the surface axial velocity increases, and the inhomogeneity is enlarged. As for the non-dimensional

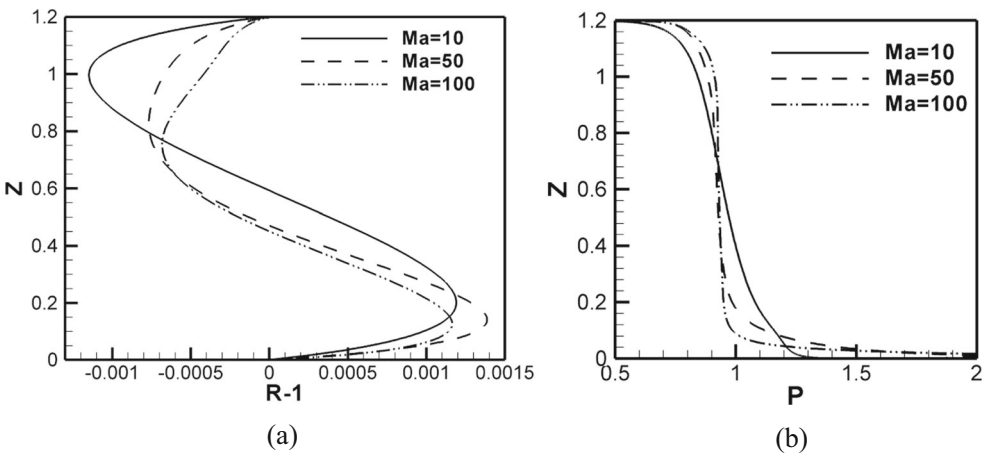

Fig. 8 Free surfaces (**a**) and surface pressure (**b**) distribution with R_σ =-10, Le = 100, Ca = 0.1 and various Ma

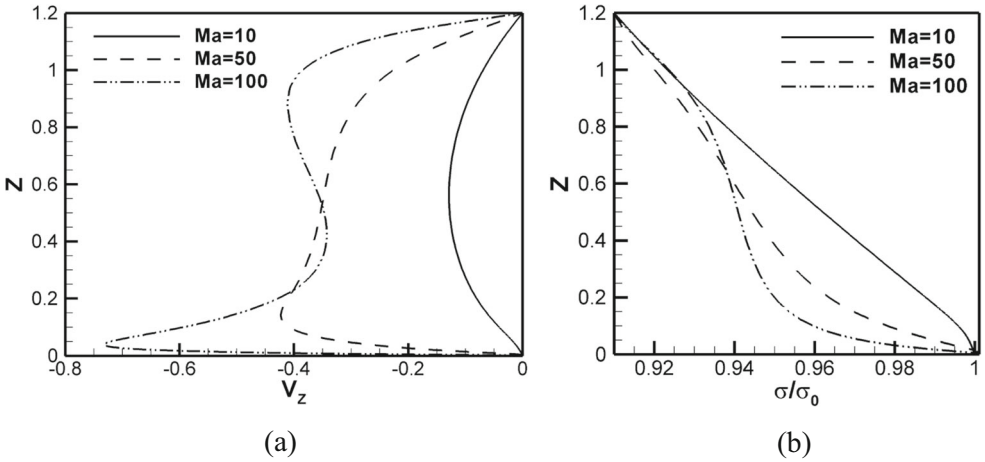

Fig. 9 Surface axial velocity (**a**) and surface tension (**b**) distribution with $R_\sigma = -10$, Le = 100, Ca = 0.1, and various Ma

surface tension, it manifests as linear variation along z axis. However, with Marangoni number increasing the distortion of the surface tension increases, particularly near the lower disk, which means the thermocapillary convection is enhanced as Marangoni number increases.

Conclusions

In this paper, steady thermo-solutocapillary convection in a liquid bridge with dynamic deformable free surface under zero gravity condition is numerically simulated, and the effects of thermal to solutal Marangoni number ratio and Marangoni number on the flow and free surface deformation are discussed. The following conclusions were drawn:

1) As $-10 \leq R_\sigma < -1$, the free surface bulges out near the lower disk and bulges in near the upper disk under low Marangoni number, and the flow field exists one anti-clockwise rotating convective cell which is driven by thermocapillary effect. With the increase of Marangoni number the free surface deformation decreases.
2) As $R_\sigma = -1$, the free surface bulges out near the lower and upper disks and bulges in at the central region of the liquid bridge under low Marangoni number, the flow field consists of one clockwise and one anti-clockwise rotating convective cells, them are driven by solutocapillary and thermocapillary convection, respectively. With the increase of Marangoni number the free surface deformation mode is changed.
3) As $-1 < R_\sigma \leq -0.01$, the free surface bulges out near the upper disk and bulges in near the lower disk, and the flow field consists of one clockwise rotating convective cell, which is driven by solutocapillary effect.

Acknowledgments This work was supported by National Natural Science Foundation of China (Grant No.51206165) and the National Basic Research Program of China (No. 2011CB710705).

References

Artemyev, V.K., Folomeev, V.I., Ginkin, V.P., Kartavykh, A.V., Mil'vidskii, M.G., Rakov, V.V.: The mechanism of Marangoni convection influence on dopant distribution in Ge space-grown single crystals. J. Cryst. Growth **223**, 2937 (2001)

Brackbill, J.U., Kothe, D.B., Zemach, C.: A continuum method for modeling surface tension. J. Comput. Phys. **100**(2), 335–354 (1992)

Joly, F., Shyy, W., Labrosse, G.: The effect of thermo-solutal capillary transport on the dynamic of liquid bridge. In: Proceedings of HT-FED04 2004 ASME Heat Transfer/Fluids Engineering Summer Conference July 11-15. Charlotte, North Carolina (2004)

Kawajia, M., Liang, R.Q., Nasr-Esfahany, M., et al.: The effect of small vibrations on Marangoni convection and the free surface of a liquid bridge. Acta. Astronautica **58**, 622–632 (2006)

Koster, J.N.: Early mission Report on the four ESA facilities: Biorack; bubble, drop and particle unit; critical point facility and advanced protein crystallization facility flown on the IML-2 spacelab mission. Microgr. News from ESA **7**, 2–7 (1994)

Kuhlmann, H.C., Nienhuser, Ch.: Dynamic free-surface deformations in thermocapillary liquid bridges. Fluid Dyn. Res. **31**, 103–127 (2002)

Levich, V.G., Krylov, V.S.: Surface-Tension-Driven Phenomena. Ann. Rev. Fluid Mech. **1**, 293–316 (1969)

Liang, R.Q., Liao, Z.Q., Jiang, W., Duan, G.D., Shi, J.Y., Liu, P.: Numerical simulation of water droplets falling near a wall: existence of wall repulsion. Microgravity Sci. Technol. **23**, 59–65 (2011)

Liang, R.Q., Ji, S.Y., Li, Z.: Thermocapillary convection in floating zone with axial magnetic fields. Microgravity Sci. Technol. **25**, 285–293 (2014)

Lin, K., Dold, P., Benz, K.W.: Numerical study of influences of buoyancy and solutal Marangoni convection on flow structures in a germanium-silicon floating zone. Cryst. Res. Technol **40**(550), 556 (2005)

Lyubimova, T.P., Skuridin, R.V., Faizrakhmanova I.S.: Effect of a magnetic field on the hysteresis transitions during floating-zone crystal growth. Tech. Phys. Lett. **33**, 744–747 (2007a)

Lyubimova, T.P., Skuridin, R.V., Faizrakhmanova, I.S.: Thermo- and soluto-capillary convection in the floating zone process in zero gravity conditions. J. Cryst. Growth **303**, 274–278 (2007b)

Lyubimova, T.P., Skuridin, R.V.: Numerical modeling of time-dependent three-dimensional flows and heat and mass transfer in a cylindrical liquid bridge in the absence of gravity. Fluid Dyn. **46**, 479–489 (2011a)

Lyubimova, T.P., Scuridyn, R.V.: Numerical modelling of three-dimensional thermo- and solutocapillary-induced flows in a floating zone during crystal growth. Eur. Phys. J. Special Topics **192**, 41–46 (2011b)

Minakuchi, H., Okano, Y., Dost, S.: A three-dimensional numerical simulation study of the Marangoni convection occurring in the crystal growth of Si_xG_{e1-x} by the float-zone technique in zero gravity. J. Cryst. Growth **266**, 140–144 (2004)

Minakuchi, H., Takagi, Y., Okano, Y., Mizoguchi, K., Gima, S., Dost, S.: A grid refinement study of half-zone configuration of the Floating Zone growth system. J. Adv. Res. Phys. **3**, 011201 (2012)

Minakuchi, H., Takagi, Y., Okano, Y., Gima, S., Dost, S.: The relative contributions of thermo-solutal Marangoni convections on flow patterns in a liquid bridge. J. Cryst. Growth **385**, 61–65 (2014)

Ni, M.J., Komori, S., Abdou, M.: A variable-density projection method for interfacial flows. Numerical Heat Tran. B **44**, 553–574 (2003)

Wanschura, M., Kuhlmann, H.C., Shevtsova, V.M., Rath, H.J.: Thermo-and solutocapillary convection in a cylindrical liquid bridge: stability of steady axisymmetric flow. Adv. Space Rev. **16**, 75–78 (1995)

Sim B.C., Kim W.S., Zebib A.: Dynamic free-surface deformations in axisymmetric liquid bridges. Adv. Space Res. **34**, 1627–1634 (2004)

Sussman, M., Smereka, P., Osher, S.: A level set approach for computing solutions to incompressible two-phase flow. J. Comput. Phys. **114**, 146–159 (1994)

Walker, J.S., Dold, P., Croll, A., Volz, M.P., Szofran, F.R.: Solutocapillary convection in the float-zone process with a strong magnetic field. Int. J. Heat Mass Tran. **45**, 4695–4702 (2002)

You, Y.R., Hu, W.R.: Analusis of thermo-solutal-capillary convection in floating zone. Chinese J. Semicond **13**, 209–2016 (1992). (in Chinese)

Zhou, X.M., Huang, H.L.: Numerical simulation of steady thermocapillary convection in a two-layer system using level set method. Microgravity Sci. Technol. **22**, 223–232 (2010)